

End-to-end Analysis and Design of a Drone Flight Controller

Zhuoqun Cheng¹, Richard West¹, and Craig Einstein¹

¹ Boston University, USA
 czq@cs.bu.edu
 richwest@cs.bu.edu
 einstein@cs.bu.edu

Abstract

Timing guarantees are crucial to cyber-physical applications that must bound the end-to-end delay between sensing, processing and actuation. For example, in a flight controller for a multirotor drone, the data from a gyro or inertial sensor must be gathered and processed to determine the attitude of the aircraft. Sensor data fusion is followed by control decisions that adjust the flight of a drone by altering motor speeds. If the processing pipeline between sensor input and actuation is not bounded, the drone will lose control and possibly fail to maintain flight.

Motivated by the implementation of a multithreaded drone flight controller on the Quest RTOS, we develop a composable pipe model based on the system’s task, scheduling and communication abstractions. This pipe model is used to analyze two semantics of end-to-end time: reaction time and freshness time. We also argue that end-to-end timing properties should be factored in at the early stage of application design. Thus, we provide a mathematical framework to derive feasible task periods that satisfy both a given set of end-to-end timing constraints and the schedulability requirement. We demonstrate the applicability of our design approach by using it to port the Cleanflight flight controller firmware to Quest on the Intel Aero board. Experiments show that Cleanflight ported to Quest is able to achieve end-to-end latencies within the predicted time bounds derived by analysis.

1998 ACM Subject Classification C.3 Real-Time and Embedded Systems

Keywords and phrases real-time systems, end-to-end timing analysis, flight controller

1 Introduction

Over the past few years, commercial and hobbyist multirotor drones have been rapidly growing in popularity. The fast development of drone technology enables an ever widening set of applications, including aerial photography [35], package delivery [3], and search and rescue [39, 27]. One of the most commonly used control boards for drones in use today is the STM32 family of systems-on-chip (SoCs), which are based on the ARM Cortex M-series processors, and include integrated inertial sensors such as a gyroscope, accelerometer and magnetometer.

While many of the existing flight control boards are perfectly adequate for drones operated via human-assisted radio control, they fall short of the processing capabilities needed for fully autonomous operation. For this reason, we are developing a new approach to building autonomous drones using emerging multicore platforms such as the Intel Aero board, Qualcomm Snapdragon flight development board [2], and Nvidia’s Jetson [1]. All these boards offer multiple processing cores and integrated graphics processing capabilities, making them capable of mission tasks that would be impossible on simpler hardware.

Our first step to building autonomous drones has so far involved a reimplementaion of the popular racing drone flight control firmware called Cleanflight [8] on the Intel Aero board. We have also ported our in-house Quest real-time OS (RTOS) [31] to the Aero board, to efficiently and predictably manage the multiple cores and I/O complexity. Our reimplementation of Cleanflight refactors the original single-threaded code running directly as firmware on STM32 SoCs into a multi-threaded application running on Quest. The decoupling of software components into separate threads improves the modularity of Cleanflight, and provides the capability for parallel task execution on platforms with multiple cores. Flight management tasks are then able to leverage the availability of increased compute resources, potentially improving the controllability of a drone. Similarly, the cleaner interfaces between software components eases our future plans to extend Cleanflight with advanced features such as camera data processing, object detection and avoidance, and simultaneous localization and mapping (SLAM) necessary for autonomous flight management.

The original Cleanflight code has a series of tasks that are executed as loops with pre-defined frequencies. These frequencies are based on a combination of the capabilities of the hardware and the experiences of drone developers. However, a multithreaded Cleanflight is subject to extra overheads and uncertainty, due to scheduling and inter-task communication. It is critical to ensure the timing correctness of Cleanflight. For example, if a gyroscope reading fails to correctly influence a change in motor (and, hence, rotor) speed within a specific time bound, the drone might not be able to stabilize.

Cleanflight is typical of many applications that process sensor inputs and require time-bounded changes to actuators. With the recent development of multi-sensor data fusion algorithms [23, 22, 17] and ever-increasing availability of open source hardware, multi-sensor/actuator cyber-physical applications are leading to a revolution in areas such as 3D printing, drones, robotics, driverless cars, and intelligent home automation systems. For these applications, it is essential to guarantee two types of end-to-end timing requirements: 1) the maximum time it takes for an input sensor reading to flow through the whole system to eventually affect an actuator output, and 2) the maximum time within which an input sensor reading remains influential on output actuator commands.

While the real-time community has developed valuable approaches to scheduling and response time analysis of tasks [10], end-to-end timing analysis has received only limited attention. Most of the prior work has originated from real-time network communication research [34, 30, 28, 40, 33, 42], and is based on event-triggered communication with FIFO-based buffers. In a drone flight control program, however, single register-based buffers and periodic sampling are more common. This paper, therefore, presents the end-to-end timing analysis of a drone flight controller based on a combination of the periodic-sampling task model, the register-based inter-task communication model and the Quest RTOS's scheduling model. We also show how the derived worst case end-to-end communication time can be, in turn, used to guide the design of applications.

Contributions of this paper include: 1) the proposal of a composable pipe model to capture the timing characteristics of end-to-end communication in the Quest RTOS; 2) a demonstration of how to derive task periods from given end-to-end timing constraints in the application design stage; 3) the re-implementation and evaluation of the Cleanflight flight controller on the Intel Aero board.

The rest of the paper is organized as follows: Section 2 provides background on Cleanflight and the corresponding task, scheduling and communication models adopted throughout the paper. Section 3 describes the end-to-end timing analysis of our proposed composable pipe model. Section 4 shows how the end-to-end time is leveraged in the application design

stage, while Section 5 details the re-implementation and evaluation of Cleanflight on the Aero board. Related work is discussed in Section 6, followed by conclusions and future work in Section 7.

2 Execution Model

In this section, we first provide an overview of the application that motivated this work. Secondly, we describe the application design model from three perspectives: *i.e.*, the task model, the scheduling model and the communication model.

2.1 Application and System Overview

This paper is motivated by our objective to implement an autonomous flight management system for multirotor drones. An autonomous drone is one that is able to reason about and adapt to changes in its surroundings, while accomplishing mission objectives without remote assistance from a human being (once its objectives are established). As part of this effort, we have undertaken a port of the Cleanflight firmware from a traditional single-core STM32-based system-on-chip (SoC) to the Intel Aero compute board. The Aero board has a quadcore x86 Atom x7-Z8750 processor, 4GB RAM, an integrated GPU, inertial measurement sensors and 3D camera connectivity. This makes it capable of flight management tasks (e.g., package delivery, aerial photography, search and rescue) that would be impossible with a less powerful single-core ARM Cortex M3 or M4 found in most STM32 SoCs.

Cleanflight is targeted at racing drones, which are operated by humans using radio control. The core software components of Cleanflight consist of sensor and actuator drivers, a PID controller, the Mahony Attitude and Heading Reference (AHRS¹) algorithm, various communication stacks, and a logging system. Runtime entities of those components are called tasks. There are 31 tasks in total, of which more than half are optional. The essential ones are listed in Table 1. Tasks are scheduled from highest to lowest dynamic priority, calculated as a function of a task’s static priority and the time since it was last executed.

Task Name	Period (μ s)	Static Priority	Description
System	100000	Medium-High	Check system utilization
Battery Alert	200000	Medium	Alarm battery runout
Battery Voltage	20000	Medium	Update battery voltage reading
Battery Current	20000	Medium	Update battery current reading
Gyro	1000	RealTime	Update gyro readings
PID	1000	RealTime	Perform PID-based motor control
Accelerometer	1000	Medium	Update accelerometer readings
IMU Attitude	10000	Medium	Calculate attitude
RC Receiver	20000	High	Process RC commands
Serial	10000	Low	Serial communication
Magnetometer	100000	Low	Update magnetometer readings

Table 1 List of Cleanflight Tasks

Our port of Cleanflight to the Aero board runs on our in-house Quest RTOS. We have developed Quest drivers for SPI, I2C, GPIO, UART, and inertial sensors on this and other similar boards. Quest is an SMP system, providing both user and kernel level threads, as

¹ The attitude is the orientation of the drone relative to a reference frame such as earth.

well as threaded interrupt handlers that are scheduled by a time-budgeted virtual CPU (VCPU) scheduler detailed in Section 2.3.

2.2 Task Model

We model the flight controller program as a set of real-time periodic tasks $\{\tau^1, \tau^2, \dots, \tau^n\}$. Each task τ^j is characterized by its worst case execution time e^j and period T^j . e^j and T^j are determined during the design stage and are fixed at runtime. e^j is usually profiled off-line under the worst case execution condition. Deciding the value of T^j is a challenging process, which is the major topic of this paper. It mainly depends on the end-to-end latency constraints and the schedulability test. All the periodic tasks are implemented using Quest's user level threads. In this paper, we use term **thread** and **task** interchangeably.

Apart from user level threads, there are kernel threads dedicated to I/O interrupts, which originate primarily from the SPI and I2C bus in Cleanflight. Quest executes interrupts in a deferrable thread context, having a corresponding time budget. This way, the handling of an interrupt does not steal CPU cycles from a currently running, potentially time-critical task.

2.3 Scheduling Model

Threads in Quest are scheduled by a two-level scheduling hierarchy, with threads mapped to virtual CPUs (VCPUs) that are mapped to physical CPUs. Each VCPU is specified a processor capacity reserve [24] consisting of a budget capacity, C , and period, T . The value of C and T are determined by the e and T of the task mapped to the VCPU. A VCPU is required to receive at least C units of execution time every T time units when it is runnable, as long as a schedulability test [20] is passed when creating new VCPUs. This way, Quest's scheduling subsystem guarantees temporal isolation between threads in the runtime environment.

Conventional periodic tasks are assigned to Main VCPUs, which are implemented as Sporadic Servers [38] and scheduled using Rate-Monotonic Scheduling (RMS) [21]. The VCPU with the smallest period has the highest priority. Instead of using the Sporadic Server model for both main tasks and bottom half threads, special I/O VCPUs are created for threaded interrupt handlers. Each I/O VCPU operates as a Priority Inheritance Bandwidth preserving Server (PIBS) [9]. A PIBS uses a single replenishment to avoid fragmentation of replenishment list budgets caused by short-lived interrupt service routines (ISRs). By using PIBS for interrupt threads, the scheduling overheads from context switching and timer reprogramming are reduced [25].

2.4 Communication Model

Control flow within the flight controller is influenced by the path of data, which originates from sensory inputs and ends with actuation. Inputs include inertial sensors, optional cameras and GPS devices, while actuators include motors that affect rotor speeds and the attitude of the drone. Data flow involves a pipeline of communicating tasks, leading to a communication model characterized by: (1) the interarrival times of tasks in the pipeline, (2) inter-task buffering, and (3) the tasks' access pattern to communication buffers.

Periodic vs. Aperiodic Tasks. Aperiodic tasks have irregular interarrival times, influenced by the arrival of data. Periodic tasks have fixed interarrival times and operate on whatever data is available at the time of their execution. A periodic task implements asynchronous communication by not blocking to await the arrival of new data [11].

Register-based vs. FIFO-based Communication. A FIFO-based shared buffer is used in scenarios where *data history* is an important factor. However, in a flight controller, *data freshness* outweighs the preservation of the full history of all sampled data. For example, the motor commands should always be computed from the latest sensor data and any stale data should be discarded. Moreover, FIFO-based communication results in loosely synchronous communication: the producer is suspended when the FIFO buffer is full and the consumer is suspended when the buffer is empty. Register-based communication achieves fully asynchronous communication between two communicating parties using Simpson’s four-slot algorithm [36].

Implicit vs. Explicit Communication. Explicit communication allows access to shared data at any time point during a task’s execution. This might lead to data inconsistency in the presence of task preemption. A task that reads the same shared data at the beginning and the end of its execution might see two different values, if it is preempted between the two reads by another task that changes the value of the shared data. Conversely, the implicit communication model [13] essentially follows a read-before-execute paradigm to avoid data inconsistency. It mandates a task to make a local copy of the shared data at the beginning of its execution and to work on that copy throughout its execution.

This paper assumes a periodic task model, as this simplifies timing analysis. Applications such as Cleanflight implement periodic tasks to sample data and perform control operations. Our system also adopts register-based, implicit communication for data freshness and consistency.

3 End-to-end Communication Timing Analysis

In this section, we first distinguish two different timing semantics for end-to-end communication, which will be used as the basis for separate timing analyses. Secondly, we develop a composable pipe model for communication, which is derived from separate latencies that influence end-to-end delay. Lastly, we use the pipe model to derive the worst case end-to-end communication time under various situations.

3.1 Semantics of End-to-end Time

To understanding the meaning of end-to-end time consider the following two constraints for a flight controller:

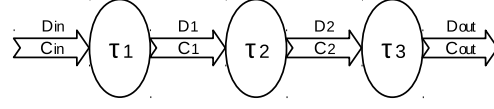
- Constraint 1: a *change* in motor speed must be within 2 ms of the gyro sensor reading that caused the change.
- Constraint 2: an *update* to a gyro sensor value must be within 2 ms of the corresponding update in motor speed.

The values before and after a *change* differ, whereas they may stay the same before and after an *update*. These semantics lead to two different constraints. To appreciate the difference, imagine the two cases in Table 2. In Case 1, the task that reads the gyro runs every 10 ms and the one that controls the motors runs every 1 ms. Case 1 is guaranteed to meet Constraint 1 because the motor task runs more than once within 2 ms, no matter whether the gyro reading changes. However, it fails Constraint 2 frequently as the gyro task is not likely to run even once in an interval of 2 ms. Conversely, Case 2 is guaranteed to meet Constraint 2 but fails Constraint 1 frequently.

This example demonstrates the difference between the two semantics of end-to-end time, which leads to the following formal definitions:

	Gyro Period	Motor Period
Case 1	10 ms	1 ms
Case 2	1 ms	10 ms

■ **Table 2** Example Periods



■ **Figure 1** Task Chain

- **Reaction time** is the time it takes for input data to flow through the system, and is affected by the period of each consumer in a pipeline. A reaction timing constraint bounds the time interval between a sensor input and the *first corresponding* actuator output.
- **Freshness time** is the time within which an instance of the input data has influence on the system, and is affected by the period of each producer in a pipeline. A freshness timing constraint bounds the time interval between a sensor input and the *last corresponding* actuator output.

Constraint 1, above, is a constraint on reaction time, while Constraint 2 is on freshness time. We perform analysis of the two semantics of time in Section 3.5.2 and 3.5.3, respectively.

3.2 Latency Contributors

The end-to-end communication delay is influenced by several factors, which we will identify as part of our analysis. To begin, we first consider the end-to-end communication pipeline illustrated as a task chain in Figure 1. Task τ_1 reads input data D_{in} over channel C_{in} , processes it and produces data D_1 . Task τ_2 reads D_1 and produces D_2 , and τ_3 eventually writes output D_{out} to channel C_{out} after reading and processing D_2 .

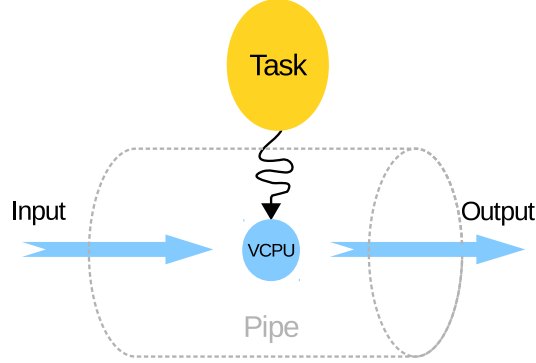
Each task handles data in three stages, *i.e.*, read, process and write. The end-to-end time should sum the latency of each stage in the task chain. Due to the asynchrony of communication, however, we also need to consider one less obvious latency, which is the waiting time it takes for an intermediate output to be read in as input, by the succeeding task in the chain. In summary, the latency contributors are classified as follows:

- **Processing latency** represents the time it takes for a task to translate a raw input to a processed output. The actual processing latency depends not only on the absolute processing time of a task without interruption, but also on the service constraints (*i.e.*, CPU budget and period of the VCPU) associated with the task.
- **Communication latency** represents the time to transfer data over a channel. The transfer data size, bandwidth and propagation delay of the communication channel, and the software overheads of the communication protocol all contribute to the overall latency. Since our communication model is asynchronous and register-based as described in Section 2, queuing latency is not a concern of this work.
- **Scheduling latency** represents the time interval between the arrival of data on a channel from a sending task and when the receiving task begins reading that data. The scheduling latency depends on the order of execution of tasks in the system, and therefore has significant influence on the end-to-end communication delay.

3.3 The Composable Pipe Model

In Section 3.2, we identified the factors that influence end-to-end communication delay. Among them, the absolute processing time and the transfer data size are determined by the

nature of the task in question. To capture the rest of the timing characteristics, we develop a composable pipe model, leveraging the scheduling approach described in Section 2.3. A task and pipe have a one-to-one relationship, as illustrated in Figure 2.



■ **Figure 2** Illustration of a Pipe

3.3.1 Terminology

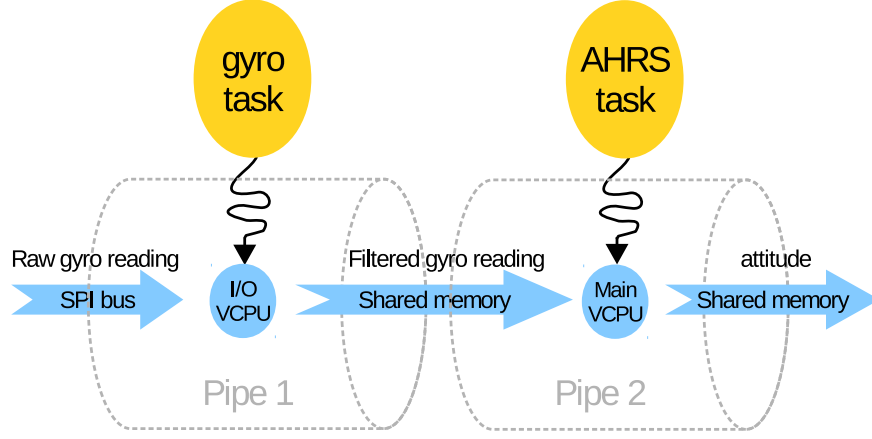
A pipe is composed of three elements:

- **Pipe Terminal.** A pipe has one terminal, which is an encapsulation of the data processing power reserved for this pipe. A pipe terminal is represented by a VCPU and its timing characteristics are captured by the VCPU’s budget and period, thereby guaranteeing at least C units of execution time every T time units. Pipe terminals are associated with conventional tasks bound to Main VCPUs and kernel control paths (including interrupt handlers and device drivers) bound to I/O VCPUs, as described in Section 2.3.
- **Pipe End.** A pipe has two ends, one for input and one for output. A pipe end is an interface to a communication channel, which is either an I/O bus or shared memory. Theoretically, the physical timing characteristics of a pipe end consist of transmission delay and propagation delay. As this work focuses on embedded systems where communicating parties are typically located within close proximity, we neglect propagation delay. The transmission delay is modeled by the bandwidth parameter, W , of the communication channel. We also use a parameter δ to denote the software overheads of a communication protocol. Though we are aware that δ depends on the data transfer size, the time difference is negligible, compared to the time of actual data transfer and processing. Therefore, for the sake of simplicity, δ is a constant in our model.

Note that in our definition of a single pipe there is only one terminal, not two at either end of the pipe. This differs from the idea of a POSIX pipe, which comprises a task at both sending and receiving ends. In our case, a pipe is represented by the single terminal that takes input and produces output.

An example of two communicating pipes is shown in Figure 3. This is representative of a communication path between a gyro task and attitude calculation in Cleanflight on the Aero board. The gyro task is mapped to Pipe 1, whose input end is over the SPI bus connected to the gyro sensor and output end is over a region of memory shared with Pipe 2. Pipe 1’s terminal is an I/O VCPU because the gyro task is responsible for handling I/O interrupts generated from the SPI bus. On the contrary, the terminal of Pipe 2 is a Main VCPU as the AHRS task is CPU-intensive. The gyro task reads raw gyro readings from Pipe 1’s input

end, processes them, and writes filtered gyro readings to Pipe 1's output end. Similarly, the AHRS task reads the filtered gyro readings from Pipe 2's input end and produces attitude data for its output end over shared memory.



■ **Figure 3** Illustration of Two Communicating Pipes

3.3.2 Notation

The timing characteristics of a pipe are denoted by the 3-tuple, $\pi = ((W_i, \delta_i), (C, T), (W_o, \delta_o))$, where:

- (W_i, δ_i) and (W_o, δ_o) denote the bandwidth and software overheads of the input and output ends, respectively.
- (C, T) denotes the budget and period of the pipe terminal.

A task τ is also represented as a 3-tuple, $\tau = (d_i, p, d_o)$, where:

- d_i denotes the size of the raw data that is read in by τ in order to perform its job, and d_o denotes the size of the processed data that is produced by τ .
- p denotes the uninterrupted processing time it takes for τ to turn the raw data into the processed data.

In addition, $\tau \mapsto \pi$ denotes the mapping between task τ and pipe π . A task $\tau = (d_i, p, d_o)$ is said to be mapped to a pipe $\pi = ((W_i, \delta_i), (C, T), (W_o, \delta_o))$ when

- data of size d_i is read from the input end with parameters (W_i, δ_i) , and data of size d_o is written to the output end with parameters (W_o, δ_o) ;
- the pipe terminal with parameters (C, T) is used for scheduling and accounting of the read and write operations, as well as the processing that takes time p .

For the composition of a chain of pipes, the operator $|$ connects a pipe's output end to its succeeding pipe's input end. For example, Figure 3 is represented as $\tau_{gyro} \mapsto \pi_1 | \tau_{AHRS} \mapsto \pi_2$. The scheduling latency between two pipes is denoted by $S_{\tau \mapsto \pi | \tau' \mapsto \pi'}$. Lastly, given a task set $T = \{\tau_1, \tau_2, \dots, \tau_n\}$ identity mapped to a pipe set $\Pi = \{\pi_1, \pi_2, \dots, \pi_n\}$, where pipes are connected to each other in ascending order of subscript, $E_{\tau_1 \mapsto \pi_1 | \tau_2 \mapsto \pi_2 | \dots | \tau_n \mapsto \pi_n}$ denotes the end-to-end reaction time of the pipe chain, and $F_{\tau_1 \mapsto \pi_1 | \tau_2 \mapsto \pi_2 | \dots | \tau_n \mapsto \pi_n}$ denotes the end-to-end freshness time.

3.4 Reachability

Before mathematically analyzing end-to-end time, we introduce the concept of **reachability**, inspired by the *data-path reachability conditions* proposed by Feiertag et al [11]. The necessity of introducing reachability is due to a subtle difference between our register-based asynchronous communication model and the traditional FIFO-based synchronous communication. In the latter, data is guaranteed to be transferred without loss or repetition. This way, end-to-end time is derived from the time interval between the arrival of a data input and the departure of its *corresponding* data output. Unfortunately, this might result in an infinitely large end-to-end time in the case of register-based asynchronous communication where not every input leads to an output. Instead, unprocessed input data might be discarded (overwritten) when newer input data is available, as explained in Section 2.4.

An infinitely large end-to-end time, while mathematically correct, lacks practical use. Therefore, the following timing analysis ignores all input data that fails to “reach” the exit of the pipe chain it enters. Instead, only those data inputs that result in data outputs from the pipe chain are considered. We define this latter class of inputs as being **reachable**.

3.5 Timing Analysis

As alluded to above, the execution of a task is divided into three stages, involving (1) reading, (2) processing, and (3) writing data. To simplify the timing analysis, we assume that tasks are able to finish the read and write stages within one period of the pipe terminal, to which the task is mapped. This is not unrealistic for applications such as a flight controller, because: 1) data to be transferred is usually small, and 2) all three stages are typically able to finish within one period. However, to maintain generality, we do not impose any restriction on the length of the processing stage.

3.5.1 Worst Case End-to-end Time of a Single Pipe

First, we consider the case where there is a single pipe. Two key observations for this case are: 1) the absence of scheduling latency due to the lack of a succeeding pipe, and 2) the equivalence of the two end-to-end time semantics (reaction and freshness time) due to the lack of a preceding pipe. We therefore use $L_{\tau \mapsto \pi}$ to unify the notation of $E_{\tau \mapsto \pi}$ and $F_{\tau \mapsto \pi}$.

Given task $\tau = (d_i, p, d_o)$ mapped to pipe $\pi = ((W_i, \delta_i), (C, T), (W_o, \delta_o))$, the worst case end-to-end time is essentially the execution time of the three stages of τ on π . Due to the timing property of π 's pipe terminal, τ is guaranteed C units of execution time within any window of T time units. Hence, the worst-case latency $L_{\tau \mapsto \pi}^{wc}$ is bounded by the following:

$$L_{\tau \mapsto \pi}^{wc} = \left\lfloor \frac{\Delta_{in} + p + \Delta_{out}}{C} \right\rfloor \cdot T + (\Delta_{in} + p + \Delta_{out}) \mod C \quad (1)$$

where $\Delta_{in} = \frac{d_i}{W_i} + \delta_i$ and $\Delta_{out} = \frac{d_o}{W_o} + \delta_o$.

3.5.2 Worst Case End-to-end Reaction Time of a Pipe Chain

In this section, we extend the timing analysis of a single pipe to a pipe chain. For the sake of simplicity, we start with a chain of length two. We show in Section 3.6 that the mathematical framework is applicable to arbitrarily long pipe chains. To distinguish the tasks mapped to the two pipes, we name the preceding task **producer** and the succeeding **consumer**. The producer is denoted by $\tau_p = (d_i^p, p^p, d)$ and its pipe is denoted by $\pi_p = ((W_i^p, \delta_i^p), (C^p, T^p), (W_o^p, \delta_o^p))$. Similarly, the consumer task and pipe are denoted by $\tau_c =$

(d, p^c, d_o^c) and $\pi_c = ((W_i^c, \delta_i^c), (C^c, T^c), (W_o^c, \delta_o^c))$. Following the definition of the end-to-end reaction time, $E_{\tau_p \mapsto \pi_p | \tau_c \mapsto \pi_c}$, in Section 3.1, we investigate the time interval between a specific instance of input data, denoted by D_i , being read by τ_p , and its **first** corresponding output, denoted by D_o , being written by τ_c .

3.5.2.1 Calculating the End-to-end Reaction Time

Case 1. The key to making use of $L_{\tau_p \mapsto \pi_p}^{wc}$ and $L_{\tau_c \mapsto \pi_c}^{wc}$ in the timing analysis of $E_{\tau_p \mapsto \pi_p | \tau_c \mapsto \pi_c}^{wc}$ is to find the worst case scheduling latency, $S_{\tau_p \mapsto \pi_p | \tau_c \mapsto \pi_c}^{wc}$. As illustrated in Figure 4, the worst case scheduling latency occurs when τ_c preempts τ_p (Step ①) immediately before τ_p produces the intermediate output D_{int} corresponding to D_i . After preemption, τ_c uses up π_c 's budget and gives the CPU back to τ_p . Upon being resumed, τ_p immediately produces D_{int} (Step ②). For τ_c to become runnable again to read D_{int} in Step ③, it has to wait for its budget replenishment. The waiting time is exactly the worst case scheduling latency:

$$S_{\tau_p \mapsto \pi_p | \tau_c \mapsto \pi_c}^{wc} = T^c - C^c - (\frac{d}{W_o^p} + \delta_o^p) \quad (2)$$

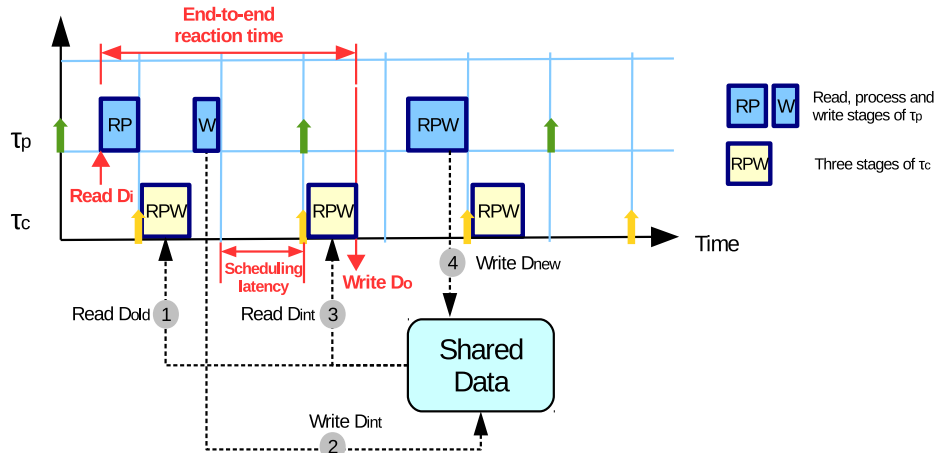


Figure 4 End-to-end Reaction Time in Case 1

After replenishment, τ_c reads in D_{int} , processes it and eventually writes out D_o . As $E_{\tau_p \mapsto \pi_p | \tau_c \mapsto \pi_c}$ is defined to be the time interval between the arrival of D_i and the departure of D_o , the worst case of $E_{\tau_p \mapsto \pi_p | \tau_c \mapsto \pi_c}$ is as follows:

$$\begin{aligned} E_{\tau_p \mapsto \pi_p | \tau_c \mapsto \pi_c}^{wc} &= L_{\tau_p \mapsto \pi_p}^{wc} + S_{\tau_p \mapsto \pi_p | \tau_c \mapsto \pi_c}^{wc} + L_{\tau_c \mapsto \pi_c}^{wc} \\ &= L_{\tau_p \mapsto \pi_p}^{wc} + L_{\tau_c \mapsto \pi_c}^{wc} + T^c - C^c - \left(\frac{d}{W_o^p} + \delta_o^p \right) \end{aligned} \quad (3)$$

Note that if τ_c runs out of budget before writing D_o , τ_p may overwrite D_{int} in the pipe with new data (Step ④). However, the *implicit communication* property guarantees that τ_c only works on its local copy of the shared data, which is D_{int} until τ_c initiates another read.

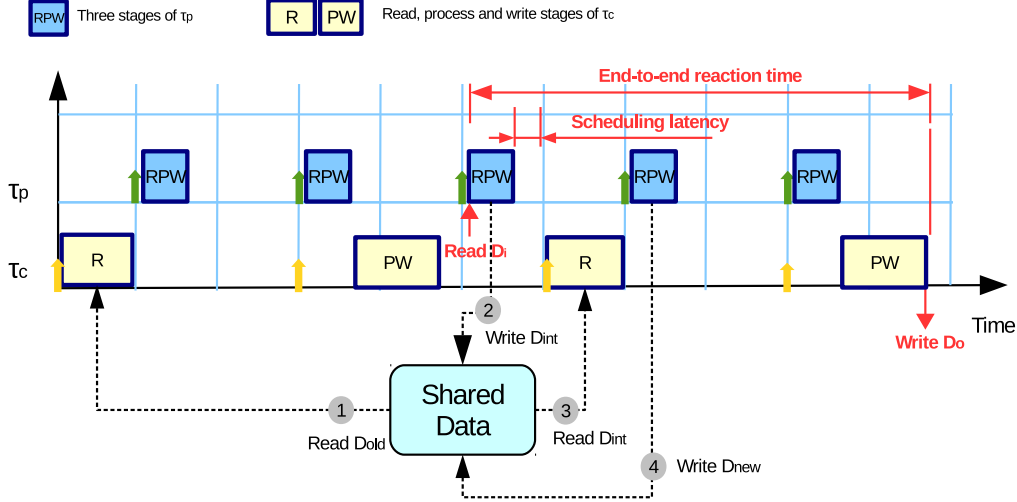


Figure 5 End-to-end Reaction Time in Case 2

Case 2. The situation is more complicated when τ_p has higher priority than τ_c . The worst case scenario in Case 1 does not hold in Case 2 primarily because τ_p might overwrite D_{int} before τ_c has a budget replenishment. This is impossible in Case 1 because τ_p has a larger period than τ_c , which is guaranteed to have its budget replenished before τ_p is able to initiate another write. In other words, in Figure 4, Step (3) is guaranteed to happen before Step (4).

The data-overwrite problem in Case 2 is the reason for introducing reachability in Section 3.4. To find the worst case end-to-end reaction time in this case, we have to find the scenario that not only leads to the worst case scheduling latency, but also originates from a **reachable** input. Figure 5 illustrates a scenario that meets these requirements. In the figure, τ_p preempts τ_c immediately after τ_c finishes reading τ_p 's intermediate output (Step (3)), D_{int} , corresponding to D_i . It follows that the longest possible waiting time, between D_{int} becoming available (Step (2)) and τ_c reading the data (Step (3)), is the period of τ_p minus both its budget and the execution time of the read stage of τ_c . This waiting time is exactly the worst case scheduling latency:

$$S_{\tau_p \mapsto \pi_p | \tau_c \mapsto \pi_c}^{wc} = T^p - C^p - \left(\frac{d}{W_i^c} + \delta_i^c \right) \quad (4)$$

Between reading D_{int} and writing D_o , τ_c might experience more than one preemption from τ_p , which repeatedly overwrites the shared data. This will not, however, affect τ_c 's processing on D_{int} either spatially or temporally, thanks to the VCPU model and the implicit communication semantic. Therefore, similar to Case 1, the worst case end-to-end reaction time is again the sum of Equation 1 of each pipe and Equation 4:

$$\begin{aligned} E_{\tau_p \mapsto \pi_p | \tau_c \mapsto \pi_c}^{wc} &= L_{\tau_p \mapsto \pi_p}^{wc} + S_{\tau_p \mapsto \pi_p | \tau_c \mapsto \pi_c}^{wc} + L_{\tau_c \mapsto \pi_c}^{wc} \\ &= L_{\tau_p \mapsto \pi_p}^{wc} + L_{\tau_c \mapsto \pi_c}^{wc} + T^p - C^p - \left(\frac{d}{W_i^c} + \delta_i^c \right) \end{aligned} \quad (5)$$

Since the output end of τ_p and the input end of τ_c share the same communication channel, it is reasonable to assume that $W_o^p = W_i^c$ and $\delta_o^p = \delta_i^c$. With that, we proceed to unify the

worst case end-to-end reaction time using one conditional equation:

$$E_{\tau_p \mapsto \pi_p | \tau_c \mapsto \pi_c}^{wc} = \begin{cases} T^c - C^c - (\frac{d}{W} + \delta) + L_{\tau_p \mapsto \pi_p}^{wc} + L_{\tau_c \mapsto \pi_c}^{wc}, & \text{if } T^c < T^p \\ T^p - C^p - (\frac{d}{W} + \delta) + L_{\tau_p \mapsto \pi_p}^{wc} + L_{\tau_c \mapsto \pi_c}^{wc}, & \text{otherwise} \end{cases} \quad (6)$$

where $W = W_o^p = W_i^c$ and $\delta = \delta_o^p = \delta_i^c$

3.5.2.2 Special Cases

Real-time systems are often profiled offline to obtain worst case execution times of their tasks. In our case, this would enable CPU resources for pipe terminals to be provisioned so that each task completes one iteration of all three stages (read, process, write) in one budget allocation and, hence, period. This implies that $\Delta_{in} + p + \Delta_{out} + \epsilon = C$ in Equation 1, where ϵ is an arbitrarily small positive number to account for surplus budget after completing all task stages. With that, it is possible to simplify the worst case end-to-end reaction time derived in Section 3.5.2.1. First, Equation 1 is simplified as follows:

$$\begin{aligned} L_{\tau \mapsto \pi}^{wc} &= \lfloor \frac{C - \epsilon}{C} \rfloor \cdot T + [(C - \epsilon) \bmod C] \\ &= 0 \cdot T + (C - \epsilon) \approx C \end{aligned} \quad (7)$$

Using Equation 7, Equation 5 reduces to:

$$\begin{aligned} E_{\tau_p \mapsto \pi_p | \tau_c \mapsto \pi_c}^{wc} &= T^p - C^p - \Delta_{in}^c + L_{\tau_p \mapsto \pi_p}^{wc} + L_{\tau_c \mapsto \pi_c}^{wc} \\ &= T^p - C^p - \Delta_{in}^c + C^p + C^c \\ &= T^p + C^c - \Delta_{in}^c \end{aligned} \quad (8)$$

The same simplification applied to Equation 3 of Case 1 reduces Equation 6 to:

$$E_{\tau_p \mapsto \pi_p | \tau_c \mapsto \pi_c}^{wc} = \begin{cases} T^c + C^p - \Delta, & \text{if } T^c < T^p \\ T^p + C^c - \Delta, & \text{otherwise} \end{cases} \quad (9)$$

where $\Delta = \frac{d}{W} + \delta$.

If we further assume that π_p and π_c communicate data of small size over shared memory, it is possible to discard communication overheads, such that $\Delta = 0$. With that, Equation 9 simplifies to:

$$E_{\tau_p \mapsto \pi_p | \tau_c \mapsto \pi_c}^{wc} = \begin{cases} T^c + C^p, & \text{if } T^c < T^p \\ T^p + C^c, & \text{otherwise} \end{cases} \quad (10)$$

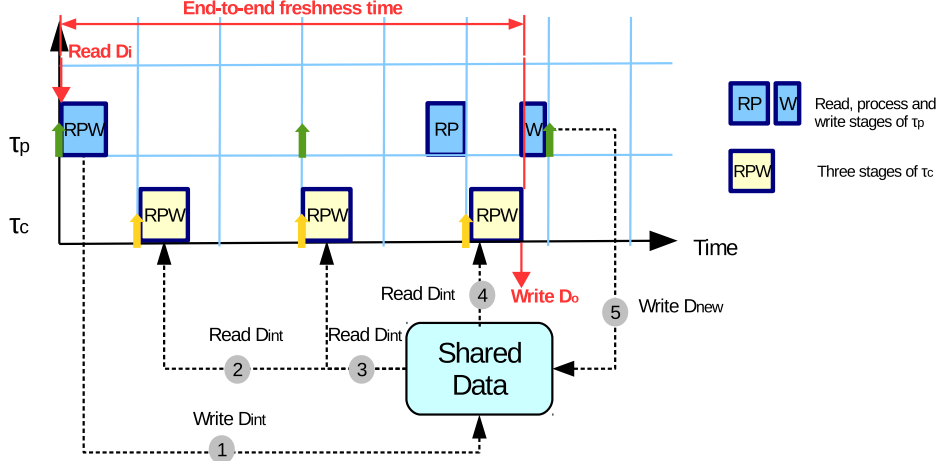
Finally, notice that by appending $\tau_c \mapsto \pi_c$ to $\tau_p \mapsto \pi_p$, the worst case end-to-end reaction time is increased by the following:

$$\begin{aligned} \uparrow E^{wc} &= E_{\tau_p \mapsto \pi_p | \tau_c \mapsto \pi_c}^{wc} - E_{\tau_p \mapsto \pi_p}^{wc} = E_{\tau_p \mapsto \pi_p | \tau_c \mapsto \pi_c}^{wc} - C^p \\ &= \begin{cases} T^c, & \text{if } T^c < T^p \\ T^p - C^p + C^c, & \text{otherwise} \end{cases} \end{aligned} \quad (11)$$

3.5.3 Worst Case End-to-end Freshness Time of a Pipe Chain

Techniques similar to those in Section 3.5.2 will be used to analyze end-to-end freshness time. To avoid repetition, we abbreviate the end-to-end freshness timing analysis by only focusing on the special cases described in Section 3.5.2.2.

Recall that freshness time is defined to be the interval between the arrival of an input and the departure of its *last corresponding* output. Therefore, we investigate the interval between a specific instance of input data, D_i , being read by τ_p and its *last* corresponding output, D_o , being written by τ_c .



■ **Figure 6** End-to-end Freshness Time in Case 1

Case 1. As illustrated in Figure 6, D_i is read by the first instance of τ_p at time 0 and the intermediate output, D_{int} , is written to the shared data (Step ①). After that, τ_c produces three outputs corresponding to D_{int} (Steps ②, ③ and ④), or to D_i indirectly. The last output, D_o , is the one preceding τ_p 's write of new data, D_{new} (Step ⑤). Thus, the worst case end-to-end freshness time, $F_{\tau_p \mapsto \pi_p | \tau_c \mapsto \pi_c}^{wc}$, occurs when: 1) the two consecutive writes (Steps ① and ⑤) from τ_p have the longest possible time interval between them, and 2) the write of D_o happens as late as possible. The latest time to write D_o is immediately before the second write of τ_p , which is preempted by higher priority τ_c .

From Figure 6 that the worst case end-to-end freshness time is:

$$F_{\tau_p \mapsto \pi_p | \tau_c \mapsto \pi_c}^{wc} = 2 \cdot T^p - \Delta_{out}^p \quad (12)$$

Again, when communicating over shared memory, Equation 12 can be further simplified to:

$$F_{\tau_p \mapsto \pi_p | \tau_c \mapsto \pi_c}^{wc} = 2 \cdot T^p \quad (13)$$

Case 2. When τ_p has a smaller period than τ_c , it is impossible for τ_c to read the same intermediate output of τ_p twice. In Figure 6, Step ⑤ is guaranteed to happen before ③. Thus, the worst case freshness time is essentially the worst case reaction time, shown in Equation 5.

In summary, the worst case end-to-end freshness latency of two communicating pipes is represented in the following conditional equation:

$$F_{\tau_p \mapsto \pi_p | \tau_c \mapsto \pi_c} = \begin{cases} 2 \cdot T^p, & \text{if } T^c < T^p \\ T^p + C^c, & \text{otherwise} \end{cases} \quad (14)$$

3.6 Composability

The timing analysis for two pipes in Section 3.5.2 extends to pipe chains of arbitrary length. Every time an extra task τ_{new} (mapped to π_{new}) is appended to the tail end of a chain

$(\tau_{tail} \mapsto \pi_{tail})$, the worst case end-to-end reaction time increases by the worst case end-to-end time of the newly appended pipe, plus the scheduling latency between the new pipe and the tail pipe. The actual value of the increase, depending on the relative priority of the new pipe and the tail pipe, is shown in Equation 11. Similarly, the added end-to-end freshness time can be derived from Equation 14.

Composability is a crucial property of our pipe model, since it significantly eases the end-to-end time calculation for any given pipeline. This provides the basis for a design framework that derives task periods from given end-to-end timing constraints. This is detailed in the following section.

4 End-to-end Design

There are significant challenges to porting a flight control firmware such as Cleanflight to run as a multithreaded application on a real-time operating system. One of the major issues is how to determine the period of each thread so that the application is able to meet its end-to-end timing constraints. A naive approach would be to start by choosing a tentative set of periods and use the timing analysis method in Section 3 to validate the timing correctness. Upon failure, the periods are heuristically adjusted and the validation step is repeated until end-to-end timing guarantees are met. This approach, however, is potentially time-consuming and labor-intensive when the number of tasks or end-to-end constraints increase.

Inspired by Gerber *et al* [12], we derive task periods from end-to-end timing constraints, by combining the timing analysis of the pipe model with linear optimization techniques. In this section, we generalize our method for use with a broader spectrum of cyber-physical control applications.

4.1 Problem Definition

To precisely define the problem, first consider a set of tasks $T = \{\tau_1, \tau_2, \dots, \tau_n\}$ and a set of pipes $\Pi = \{\pi_1, \pi_2, \dots, \pi_n\}$, where $\tau_j = (d_i^j, p^j, d_o^j)$ and $\pi_j = ((W_i^j, \delta_i^j), (C^j, T^j), (W_o^j, \delta_o^j))$. We additionally require the following information:

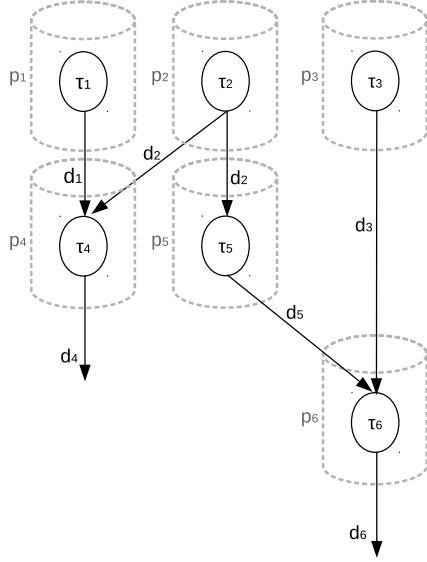
- the mapping between T and Π . For ease of notation, we assume tasks map to the pipe with the same subscript, hence $\forall j \in \{1, 2, \dots, n\}, \tau_j \mapsto \pi_j$;
- the topology of Π (an example is shown in Figure 7);
- $\forall j \in \{1, 2, \dots, n\}$, the value of d_i^j , p^j and d_o^j ;
- $\forall j \in \{1, 2, \dots, n\}$, the value of W_i^j , δ_i^j , W_o^j and δ_o^j ;
- the end-to-end timing constraints, namely the value of $E_{\tau_i \mapsto \pi_i | \tau_j \mapsto \pi_j | \dots | \tau_k \mapsto \pi_k}$ and/or $F_{\tau_p \mapsto \pi_p | \tau_q \mapsto \pi_q | \dots | \tau_r \mapsto \pi_r}$ where $i, j, k, p, q, r \in \{1, 2, \dots, n\}$.

The aim is to find a feasible set of $\{(C^j, T^j)\}$ pairs for $j \in \{1, 2, \dots, n\}$ that:

1. meets all the specified end-to-end timing constraints,
2. passes the task schedulability test, and
3. ideally but not necessarily minimizes CPU utilization. A task should not be run faster than it needs to be, so that resources are made available for additional system objectives.

4.2 Solving the Constraints

Our solution is carried out in a three-step process. To make it easier to understand, we use a concrete example with actual numbers to elaborate the process. Consider the pipe topology



■ **Figure 7** Application Task Graph

$ \begin{aligned} E_{\tau_1 \mapsto \pi_1 \tau_4 \mapsto \pi_4} &\leq 10, \\ E_{\tau_2 \mapsto \pi_2 \tau_4 \mapsto \pi_4} &\leq 15, \\ E_{\tau_2 \mapsto \pi_2 \tau_5 \mapsto \pi_5 \tau_6 \mapsto \pi_6} &\leq 25, \\ E_{\tau_3 \mapsto \pi_3 \tau_6 \mapsto \pi_6} &\leq 15; \end{aligned} $	Reaction
$ \begin{aligned} F_{\tau_1 \mapsto \pi_1 \tau_4 \mapsto \pi_4} &\leq 20, \\ F_{\tau_2 \mapsto \pi_2 \tau_4 \mapsto \pi_4} &\leq 30, \\ F_{\tau_2 \mapsto \pi_2 \tau_5 \mapsto \pi_5 \tau_6 \mapsto \pi_6} &\leq 50, \\ F_{\tau_3 \mapsto \pi_3 \tau_6 \mapsto \pi_6} &\leq 20; \end{aligned} $	Freshness
$\sum_{j=1}^6 \frac{C^j}{T^j} \leq n(\sqrt[6]{2} - 1)$	Schedulability
$ \begin{aligned} \forall j \in \{1, 2, \dots, 6\}, \\ d_i^j = d_o^j = 3, \\ W_i^j = W_o^j = 20, \\ \delta_i^j = \delta_o^j = 0.1, \\ p^j = 0.5; \end{aligned} $	Execution Times

■ **Table 3** Application Timing Characteristics

graph shown in Figure 7, in which there are six tasks mapped to six pipes. Tasks 1, 2 and 3 read inputs from sensors, Tasks 4 and 6 write their outputs to actuators, and Task 5 is an intermediary responsible for complicated processing such as PID control or sensor data fusion. The timing characteristics of the tasks and pipes are shown in Table 3. Note that the execution times are assumed to be identical for all tasks. In practice this would not necessarily be the case but it does not affect the generality of the approach.

In Step 1, we use the given d_i , d_o , p , W_i , δ_i , W_o and δ_o to compute the budget of each pipe terminal. The budget is set to a value that ensures the three stages (*i.e.*, read, process and write) finish in one period. To compute C^1 , for example, we aggregate the times for τ_1 to read, process and write data. Thus $C^1 = \frac{d_i^1}{W_i^1} + \delta_i^1 + p^1 + \frac{d_o^1}{W_o^1} + \delta_o^1$. All budgets are computed in a similar way. When the input to a pipe terminal comes from multiple sources the value d_i is aggregated from all input channels. For example, τ_4 receives a maximum of $d_i^4 = d_1 + d_2$ amount of data every transfer from both τ_1 and τ_2 . Data from a pipe terminal is not necessarily duplicated for all pipe terminals that are consumers. For example, τ_2 generates a maximum of $d_o^2 = d_2$ amount of data every transfer, by placing a single copy of the output in a shared memory region accessible to both τ_4 and τ_5 . If the communication channels did not involve shared memory, then data would be duplicated, so that $d_o^2 = 2d_2$.

In Step 2, we derive a list of inequations involving period variables from the given end-to-end timing and scheduling constraints in Table 3. For simplicity, the scheduling constraint is shown as a rate-monotonic utilization bound on the six pipe tasks. However, for sensor inputs and some actuator outputs, our system would map those tasks to I/O VCPUs that have a different utilization bound, as described in our earlier work [9]. The derivation is based on Equations 9 and 14, and the composability property of the pipe model. According to the conditional equations, however, every two pipes with undetermined priority can lead to two possible inequations. This exponentially increases the search space for feasible periods. In order to prune the search space, our strategy is to always start with the case where $T^p > T^c$.

This is based on the observation that tasks tend to over-sample inputs for the sake of better overall responsiveness. Thus, the reaction constraint $E_{\tau_2 \mapsto \pi_2 | \tau_5 \mapsto \pi_5 | \tau_6 \mapsto \pi_6} \leq 25$, for example, is translated to inequation $T^5 + C^2 - \Delta + T^6 \leq 25$. This is derived by combining Equations 9 and 11. It is then possible to translate all timing constraints to inequations with only periods as variables. In addition, periods are implicitly constrained by $T^j > C^j, \forall j \in \{1, 2, \dots, n\}$.

Given all the inequations, Step 3 attempts to find the maximum value for each period so that the total CPU utilization is minimized. We are then left with a linear programming problem. Unfortunately, there is no polynomial time solution to the integer linear programming problem, as it is known to be NP-hard. Though linear programming solutions are still available under certain mathematical conditions [4], this is beyond the scope of this paper. Instead, in practice, the problem can be simplified because 1) there are usually a small number of fan-in and fan-out pipe ends for each task, meaning that a period variable is usually involved in a small number of inequations, and 2) a sensor task period is usually pre-determined by a hardware sampling rate limit. For example, if we assume T^3 is known to be 5, a feasible set of periods for the example in Table 3 is easily found: $\{T^1 = 10, T^2 = 15, T^3 = 10, T^4 = 10, T^5 = 15, T^6 = 5\}$. If we ignore the integer requirement, it is possible to find a feasible solution in polynomial time using rational numbers that are rounded to integers. Though rounding may lead to constraint violations, it is possible to increase the time resolution to ensure system overheads exceed those of rounding errors. In the worst case, the designer is always able to perform an exhaustive search of all possible constraint solutions.

5 Evaluation

This section describes both simulations and experiments on the Intel Aero board with an Atom x7-Z8750 1.6 GHz 4-core processor and 4GB RAM.

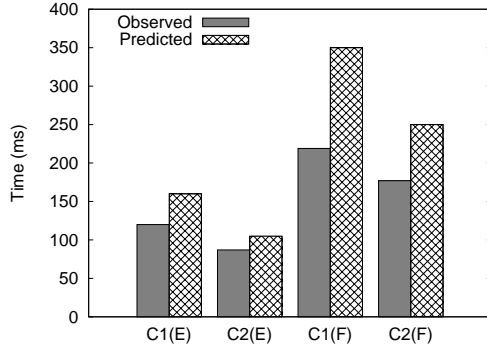
5.1 Simulation Experiments

We developed simulations for both Linux and Quest, to predict the worst-case end-to-end time using the equations in Section 3. Each simulation consists of three tasks, τ_1, τ_2 and τ_3 , mapped to pipes, π_1, π_2 and π_3 , respectively. All three tasks search for prime numbers within a certain range and then communicate with one another to exchange their results. τ_1 communicates with τ_2 , which further communicates with τ_3 . The communication channel is shared memory with caches disabled and the data size is set to 6.7 KB to achieve a non-negligible 1 millisecond communication overhead. Each task is assigned a different search range and the profiled execution time is shown in Table 4 in milliseconds. The budget of each pipe is set to be slightly larger than the execution time of its corresponding task, to compensate for system overheads. The settings of each pipe terminal (PT) are also shown in Table 4, again in milliseconds. Apart from the three main tasks, the system is loaded with low priority background tasks that consume all the remaining CPU resources and serve as potential interferences.

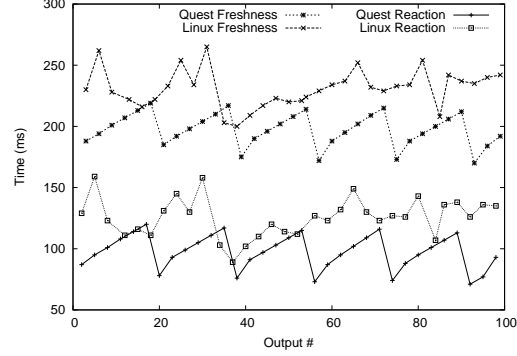
	PT 1	PT 2	PT 3	τ_1	τ_2	τ_3
Case 1	(10,50)	(10,150)	(5,100)	9.5	9.5	4.5
Case 2	(5,100)	(10,50)	(10,150)	4.5	9.5	9.5

■ **Table 4** Simulation Settings

For each case, we measure the end-to-end reaction time and freshness time separately and compare them to corresponding theoretical bounds. Figure 8 shows the results after 100,000 outputs are produced by τ_3 . $C1(E)$ and $C1(F)$ are the end-to-end reaction and freshness times, respectively, for Case 1 in Table 4, while $C2(E)$ and $C2(F)$ are for Case 2. As can be seen, the observed values are always within the prediction bounds. As reference, we also perform the two cases on Yocto Linux shipped with the Aero board. The kernel is version 4.4.76 and patched with the PREEMPT_RT patch. While running the simulation, the system also uncompresses Linux source code in the background. This places the same load on the system as the background tasks in Quest. Figure 9 shows all (not only worst case) end-to-end reaction and freshness times within the first 100 outputs. Compared to Linux, there is less variance shown by the end-to-end times on Quest. Additionally, the freshness and reaction times are generally lower with Quest than Linux. Figure 11 summarizes the worst case reaction time (WCR), maximum variance of WCR (MaxRV), worst case freshness time (WCF) and maximum variance of WCF (MaxFV) for both Quest and Linux.



■ Figure 8 Observed vs. Predicted



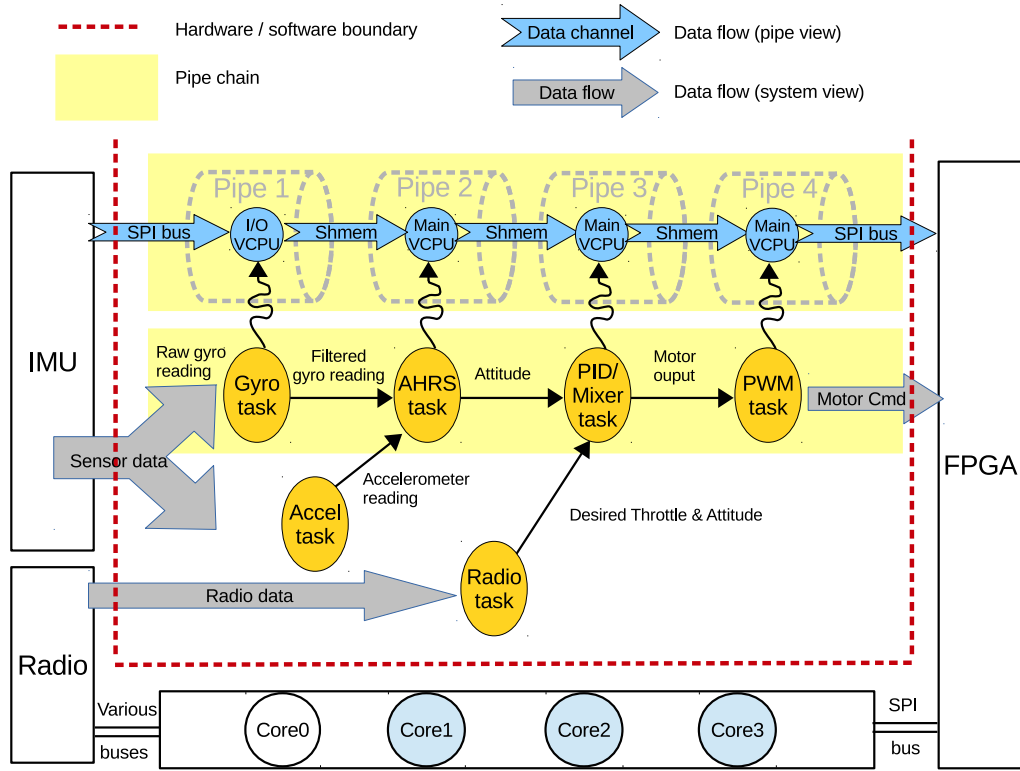
■ Figure 9 Quest vs. Linux

5.2 The Cleanflight Experiment

Our next experiments apply the end-to-end design approach to determining the periods of each task in the re-implementation of Cleanflight. We decouple software components in the original Cleanflight firmware and re-build the flight controller as a multithreaded application running on the Intel Aero board. The hardware and software architecture is shown in Figure 10.

Hardware. We currently only use Core 0 to run Cleanflight on Quest. The remaining three cores are reserved for our Quest-V separation kernel [41] to run a general purpose OS such as Linux. Apart from the main processor, the Aero board also has an FPGA-based I/O coprocessor. It provides FPGA-emulated I/O interfaces including analog-to-digital conversion (ADC), UART serial, and pulse-width modulation (PWM). Our system currently uses the I/O hub to send PWM signals to electronic speed controllers (ESCs) that alter motor and, hence, rotor speeds of the drone. We modified the FPGA logic to improve the timing resolution of PWM signals, as well as control their duty cycle and periods. We make additional use of an onboard Bosch BMI160 Inertial Measurement Unit (IMU). Both the I/O hub and the IMU are connected to the main processor via SPI bus.

Software. To minimize the engineering efforts, we currently disable the auxiliary features of Cleanflight such as telemetry, blackbox data logging, and UART-based flight control configuration. The essential components are shown as circular tasks in Figure 10. The



■ **Figure 10** Cleanflight Data Flow

AHRS sensor fusion task takes the input readings of the accelerometer and gyroscope (in the BMI160 IMU) and calculates the current attitude of the drone. Then, the PID task compares the calculated and target attitudes, and feeds the difference to the PID control logic. In the original Cleanflight code, the target attitude is determined by radio-control signals from a human flying the drone. In an autonomous setting, the target attitude would be calculated according to on-board computations based on mission objectives and flight conditions. The output is nonetheless mixed with the desired throttle and read in by the PWM task, which translates it to motor commands. Motor commands are sent over the SPI bus and ultimately delivered as PWM signals to each ESC associated with a separate motor-rotor pair on the multirotor drone. We decouple all these tasks into separate threads. For safety reasons, the sensor tasks and the PWM task are given individual address spaces. To simplify the experiment setup, we instrument Cleanflight to use a synthetic radio input value (20% throttle and 0 degree pitch, roll, and yaw angle) instead of reading from the real radio driver. The tasks are profiled and execution times are shown in Table 5.

	Gyro	AHRS	PID	PWM	Accl	Radio
Exec Times (μ s)	174	10	2	970	167	12

■ **Table 5** Task Execution Times

As can be seen in Figure 10, there are currently three data paths, originating from the gyro, the accelerometer and the radio receiver, respectively. Unfortunately, there is little information available on what end-to-end timing constraints should be imposed on each path to guarantee a working drone. Most timing parameters in the original Cleanflight are

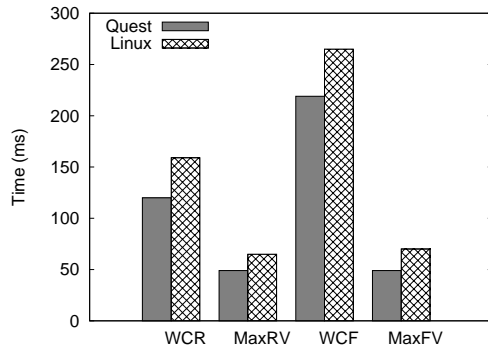
determined by trial and error. On the other hand, instead of determining the optimum timing constraints, the focus of this paper is on guaranteeing given constraints. Therefore, we first port Cleanflight to Yocto Linux on the Aero board, as a reference implementation. The Linux version remains single-threaded and used to estimate the desired end-to-end time. For example, for the gyro path, the worst case reaction and freshness times are measured to be 9769 and 22972 μs , respectively. We round them to 10 and 23 ms, and use them as end-to-end timing constraints for the Quest flight controller implementation. Using the same approach, we determine end-to-end reaction and freshness times for the accelerometer path, which are set to 10 and 23 ms, respectively. Finally, for the radio path, we set the end-to-end reaction and freshness times to be 20 and 44 ms, respectively.

Using the execution times in Table 5 and timing constraints above, we apply the end-to-end design approach to derive the periods. The results for each task are shown in Table 6.

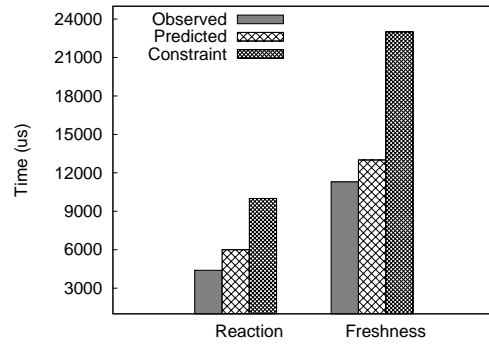
	Gyro	AHRS	PID	PWM	Acc1	Radio
Budget/Period (μs)	200/1000	100/5000	100/2000	1000/5000	200/1000	100/10000

■ **Table 6** Task Periods

Evaluation. To measure the actual end-to-end time, we focus on the longest pipe chain highlighted in Figure 10. We instrument the Cleanflight code to append every gyro reading with an incrementing ID, and also record a timestamp before the gyro input is read. The timestamp is then stored in an array indexed by the ID. Every task is further instrumented to maintain the ID when translating input data to output. This way, the ID is preserved along the pipe chain, from the input gyro reading to the output motor command. After the PWM task sends out motor commands, it looks up the timestamp using its ID and compares it to the current time. By doing this, we are able to log both the reaction and freshness end-to-end time for every input gyro reading. We then compare the observed end-to-end time with the given timing constraints, as well as the predicted worst case value. Results are shown in Figure 12. As can be seen, the observed values are always within the predicted bounds, and always meet the timing constraints.



■ **Figure 11** Quest vs. Linux Worst-Case Times



■ **Figure 12** Cleanflight Times

6 Related Work

Feiertag *et al.* [11] distinguish four semantics of end-to-end time and provides a generic framework to determine all the valid data paths for each semantic. The authors do not

perform timing analysis as no scheduling model is assumed. Hamann *et al.* also discuss end-to-end reaction and age time [13]. Their work focuses on integrating three different communication models, including the implicit communication model, into existing timing analysis tools such as SymTA/S [14]. While our composable pipe model is also based on implicit communication, we perform timing analysis using the Quest RTOS's task and scheduling model. A large portion of end-to-end reaction time analysis is based on the synchronous data-flow graph (SDFG) [19] where inter-task communication is driven by the arrival of input data. In recent work [37], Singh *et al.* enhance the standard SDFG to allow the specification of an end-to-end latency constraint.

Gerber *et al.* [12] propose a synthesis approach that determines tasks' periods, offsets and deadlines from end-to-end timing constraints. Their work relies on task precedence constraints as there is no scheduling model used for the analysis. Our work uses a scheduling model based on Quest to perform end-to-end timing analysis. We then derive task periods and budgets to ensure specific reaction, freshness and schedulability constraints.

There are also efforts to develop programming languages, such as Prelude [29] and Giotto [15], which are able to derive tasks' periods based on user-specified timing constraints. Kirsch *et al.* [18] use Giotto to reimplement a helicopter control system. Others have developed data-triggered rather than time-triggered drone flight control using reactive programming languages [5].

In general operating systems, Scout [26] exposes paths that are similar to pipe chains in our model, to offer Quality of Service guarantees to applications. Paths in Scout are non-preemptive schedulable entities ordered according to an EDF policy.

Lastly, programming environments such as ROS [32], OROCOS [6] and LCM [16], already widely adopted in the design of robotics and autonomous cars, are changing the development of cyber-physical applications. Publisher-subscriber paradigms used by ROS, for example, have influenced our thinking in the design cyber-physical systems with modularity and robustness amongst software components. We aim to augment Cleanflight functionality with ROS-style services as part of our ongoing efforts to build autonomous drones.

7 Conclusions and Future Work

In this paper, we identify two semantics of end-to-end time, namely reaction and freshness time. We analyze them in the context of the Quest RTOS, for a port of the well-known Cleanflight flight control firmware implemented as a collection of user-level tasks. This paper describes a composable pipe model that is built on task, scheduling and communication abstractions. Using the pipe model, we derive the worst case end-to-end time for data flow through a chain of tasks under various conditions. We argue that end-to-end timing properties should be factored in at the early stage of application design. Thus, we provide a mathematical framework to derive feasible task periods and budgets using the Quest scheduling framework to satisfy a given set of end-to-end timing and schedulability constraints. We demonstrate the applicability of our design approach by using it to port the Cleanflight flight controller to Quest on the Intel Aero board.

Future work will integrate the end-to-end design approach into our Quest-Arduino (Qduino [7]) development environment. This will provide the basis for the design and implementation of an autonomous multicore flight management system on our Quest-V separation kernel [41]. Quest-V enables non-time-critical tasks to run on a legacy Linux system in parallel with real-time tasks running on our Quest RTOS.

References

- 1 Nvidia Jetson Board, March 2017. <http://www.nvidia.com/object/embedded-systems.html>.
- 2 Qualcomm Snapdragon Flight Kit, March 2017. <https://www.intrinsyc.com/vertical-development-platforms/qualcomm-snapdragon-flight/>.
- 3 Amazon Prime Air. <http://www.amazon.com/b?ie=UTF8&node=8037720011>.
- 4 S.P. Bradley, A.C. Hax, and T.L. Magnanti. *Applied Mathematical Programming*. Addison-Wesley Publishing Company, 1977.
- 5 Endri Bregu, Nicola Casamassima, Daniel Cantoni, Luca Mottola, and Kamin Whitehouse. Reactive Control of Autonomous Drones. In *Proceedings of the 14th Annual International Conference on Mobile Systems, Applications, and Services*, MobiSys '16, pages 207–219, New York, NY, USA, 2016. ACM.
- 6 H. Bruyninckx. Open Robot Control Software: the OROCOS Project. In *Proceedings 2001 ICRA. IEEE International Conference on Robotics and Automation (Cat. No.01CH37164)*, volume 3, pages 2523–2528 vol.3, 2001.
- 7 Zhuoqun Cheng, Ye Li, and Richard West. Qduino: A Multithreaded Arduino System for Embedded Computing. In *Proceedings of the 2015 IEEE Real-Time Systems Symposium (RTSS)*, RTSS '15, pages 261–272, Washington, DC, USA, 2015. IEEE Computer Society.
- 8 Cleanflight: <http://cleanflight.com/>.
- 9 Matthew Danish, Ye Li, and Richard West. Virtual-CPU Scheduling in the Quest Operating System. In *Proceedings of the 17th Real-Time and Embedded Technology and Applications Symposium*, 2011.
- 10 Robert I. Davis, Sebastian Altmeyer, Leandro Indrusiak, Claire Maiza, Vincent Nelis, and Jan Reineke. An Extensible Framework for Multicore Response Time Analysis. *Real-Time Systems*, 2017.
- 11 Nico Feiertag, Kai Richter, Johan Nordlander, and Jan Jonsson. A Compositional Framework for End-to-End Path Delay Calculation of Automotive Systems under Different Path Semantics. In *Proceedings of the IEEE Real-Time System Symposium - Workshop on Compositional Theory and Technology for Real-Time Embedded Systems, Barcelona, Spain*, November 30, 2008.
- 12 Richard Gerber, Seongsoo Hong, and Manas Saksena. Guaranteeing Real-Time Requirements With Resource-Based Calibration of Periodic Processes. *IEEE Trans. Softw. Eng.*, July 1995.
- 13 Arne Hamann, Dakshina Dasari, Simon Kramer, Michael Pressler, and Falk Wurst. Communication Centric Design in Complex Automotive Embedded Systems. In *29th Euromicro Conference on Real-Time Systems (ECRTS 2017)*, Leibniz International Proceedings in Informatics (LIPIcs), Dagstuhl, Germany, 2017.
- 14 Rafik Henia, Arne Hamann, Marek Jersak, Razvan Racu, Kai Richter, and Rolf Ernst. System Level Performance Analysis - the SymTA/S Approach. In *IEEE Proceedings Computers and Digital Techniques*, 2005.
- 15 Thomas A. Henzinger, Benjamin Horowitz, and Christoph Meyer Kirsch. *Giotto: A Time-Triggered Language for Embedded Programming*, pages 166–184. Springer Berlin Heidelberg, Berlin, Heidelberg, 2001.
- 16 Albert S. Huang, Edwin Olson, and David Moore. LCM: Lightweight Communications and Marshalling. In *Proceedings of the IEEE/RSJ International Conference on Intelligent Robots and Systems (IROS)*, Taipei, Oct 2010.
- 17 Jonathan Kelly and Gaurav S Sukhatme. Visual-Inertial Sensor Fusion: Localization, Mapping and Sensor-to-Sensor Self-calibration. *The International Journal of Robotics Research*, 30(1):56–79, 2011.

- 18 Christoph M. Kirsch, Marco A. A. Sanvido, Thomas A. Henzinger, and Wolfgang Pree. *A Giotto-Based Helicopter Control System*, pages 46–60. Springer Berlin Heidelberg, Berlin, Heidelberg, 2002.
- 19 E. A. Lee and D. G. Messerschmitt. Synchronous data flow. *Proceedings of the IEEE*, 75(9):1235–1245, Sept 1987.
- 20 John Lehoczky, Lui Sha, and Ye Ding. The Rate Monotonic Scheduling Algorithm: Exact Characterization and Average Case Behavior. In *Proceedings of the IEEE Real-Time Systems Symposium (RTSS)*, 1989.
- 21 C. L. Liu and James W. Layland. Scheduling Algorithms for Multiprogramming in a Hard Real-Time Environment. *Journal of the ACM*, 20(1):46–61, 1973.
- 22 Sebastian O.H. Madgwick. An Efficient Orientation Filter for Inertial and Inertial/Magnetic Sensor Arrays. Technical report, University of Bristol, 2010.
- 23 Robert Mahony, Tarek Hamel, and Jean-Michel Pflimlin. Nonlinear Complementary Filters on the Special Orthogonal Group. *IEEE Transactions on Automatic Control*, 53, June 2008.
- 24 Clifford W. Mercer, Stefan Savage, and Hideyuki Tokuda. Processor Capacity Reserves for Multimedia Operating Systems. Technical report, Pittsburgh, PA, USA, 1993.
- 25 E. Missimer, K. Missimer, and R. West. Mixed-Criticality Scheduling with I/O. In *28th Euromicro Conference on Real-Time Systems (ECRTS)*, pages 120–130, July 2016.
- 26 David Mosberger and Larry L. Peterson. Making Paths Explicit in the Scout Operating System. In *Proceedings of the Second USENIX Symposium on Operating Systems Design and Implementation*, OSDI '96, pages 153–167, New York, NY, USA, 1996. ACM.
- 27 BBC News. Disaster Drones: How Robot Teams can Help in a Crisis. goo.gl/6effiV.
- 28 R. S. Oliver and G. Fohler. Probabilistic Estimation of End-to-end Path Latency in Wireless Sensor Networks. In *2009 IEEE 6th International Conference on Mobile Adhoc and Sensor Systems*, pages 423–431, Oct 2009.
- 29 Claire Pagetti, Julien Forget, Frédéric Boniol, Mikel Cordovilla, and David Lesens. Multi-task Implementation of Multi-periodic Synchronous Programs. *Discrete Event Dynamic Systems*, Sep 2011.
- 30 Bo Peng, Nathan Fisher, and Thidapat Chantem. MILP-based Deadline Assignment for End-to-End Flows in Distributed Real-Time Systems. In *Proceedings of the 24th International Conference on Real-Time Networks and Systems*, RTNS '16, pages 13–22, New York, NY, USA, 2016. ACM.
- 31 Quest RTOS: <http://questos.org/>.
- 32 Morgan Quigley, Ken Conley, Brian P. Gerkey, Josh Faust, Tully Foote, Jeremy Leibs, Rob Wheeler, and Andrew Y. Ng. ROS: An Open-source Robot Operating System. In *ICRA Workshop on Open Source Software*, 2009.
- 33 S. Quinton, T. T. Bone, J. Hennig, M. Neukirchner, M. Negrean, and R. Ernst. Typical Worst Case Response-time Analysis and its use in Automotive Network Design. In *2014 51st ACM/EDAC/IEEE Design Automation Conference (DAC)*, pages 1–6, June 2014.
- 34 J. L. Scharbarg, F. Ridouard, and C. Fraboul. A Probabilistic Analysis of End-To-End Delays on an AFDX Avionic Network. *IEEE Transactions on Industrial Informatics*, 5(1):38–49, Feb 2009.
- 35 Da-Jiang Innovations Science and Technology Co. DJI. <http://dji.com/>.
- 36 H.R. Simpson. Four-slot Fully Asynchronous Communication Mechanism. *IEEE Computers and Digital Techniques*, 137:17–30, January 1990.
- 37 Abhishek Singh, Pontus Ekberg, and Sanjoy Baruah. Applying Real-Time Scheduling Theory to the Synchronous Data Flow Model of Computation. In *29th Euromicro Conference on Real-Time Systems (ECRTS 2017)*, Leibniz International Proceedings in Informatics (LIPIcs), Dagstuhl, Germany, 2017.

- 38 B. Sprunt. Scheduling Sporadic and Aperiodic Events in a Hard Real-Time System. Technical Report CMU/SEI-89-TR-011, Software Engineering Institute, Carnegie Mellon, 1989.
- 39 K. P. Valavanis. *Advances in Unmanned Aerial Vehicles*. Springer Science and Business Media, 2008.
- 40 Y. Wang, M. C. Vuran, and S. Goddard. Cross-Layer Analysis of the End-to-End Delay Distribution in Wireless Sensor Networks. In *2009 30th IEEE Real-Time Systems Symposium*, pages 138–147, Dec 2009.
- 41 Richard West, Ye Li, Eric Missimer, and Matthew Danish. A Virtualized Separation Kernel for Mixed-Criticality Systems. *ACM Trans. Comput. Syst.*, 34(3):8:1–8:41, June 2016.
- 42 P. M. Yomsi, D. Bertrand, N. Navet, and R. I. Davis. Controller Area Network (CAN): Response Time Analysis with Offsets. In *2012 9th IEEE International Workshop on Factory Communication Systems*, pages 43–52, May 2012.